Journal of Materials Chemistry A

PAPER

View Article Online
View Journal | View Issue

Cite this: J. Mater. Chem. A, 2015, 3, 1972

Initial decomposition reaction of di-tetrazine-tetroxide (DTTO) from quantum molecular dynamics: implications for a promising energetic material†

Cai-Chao Ye,[ab] Qi An,[a] William A. Goddard III,*[a] Tao Cheng,[a] Wei-Guang Liu,[a] Sergey V. Zybin[a] and Xue-Hai Ju[b]

Received 23rd October 2014
Accepted 12th November 2014

DOI: 10.1039/c4ta05676k

www.rsc.org/MaterialsA

Di-tetrazine-tetroxide (DTTO) was predicted in 2001 to have a density (up to 2.3 g cm^{-3}) and heat of detonation (up to 421.0 kcal mol^{-1}) better than other explosives, making it the "holy grail" of energetic materials (EMs), but all attempts at synthesis have failed. We report Density Functional Theory (DFT) molecular dynamics simulations (DFT-MD) on DTTO crystal for the two most stable monomers. We predict that the most stable isomer (c1) has a density of $\rho = 1.96$ g cm^{-3} with an estimated detonation velocity (D_v) of 9.70 km s^{-1} and a detonation pressure (D_p) of 43.0 GPa, making it comparable to RDX ($\rho = 1.82$ g cm^{-3}, $D_v = 8.75$ km s^{-1}, $D_p = 35.0$ GPa), HMX ($\rho = 1.91$ g cm^{-3}, $D_v = 9.10$ km s^{-1}, $D_p = 39.3$ GPa) and CL-20 ($\rho = 2.04$ g cm^{-3}, $D_v = 9.38$ km s^{-1}, $D_p = 44.1$ GPa). The DFT-MD studies find that the initial reaction at lower pressure is unimolecular decomposition to form two N_2O molecules (barrier 45.9 kcal mol^{-1}), while at higher pressure it is intermolecular oxygen-transfer with a barrier of 40.1 kcal mol^{-1}. For the c2 isomer (less stable by 1.2 kcal mol^{-1}) the initial reaction involves two DTTO molecules reacting to form a dimer which then releases N_2 as a direct product (barrier 48.1 kcal mol^{-1}), a unique initial reaction among EMs. These results suggest that DTTO may have a higher thermal stability (barrier >7.0 kcal mol^{-1} higher) than RDX, HMX, and CL-20.

1. Introduction

The last decade has seen tremendous progress in using quantum mechanics (QM) to predict the detailed reaction barriers and kinetics of gas phase bimolecular and unimolecular reactions with detailed confirmation from experiment and concomitant interpretation of experiment.[1–9] In addition, the last few years has seen similar progress in predicting and explaining the detailed reaction mechanisms, selectivity, and activity of organometallic reactions in solvents that have guided experiment and been confirmed by experiment.[10–13] There has also been significant progress in explaining key aspects of heterogeneous catalysts that have helped somewhat with guiding experiment with some confirmation from experiment.[14–16] However, progress has been much more limited in bulk phase reaction mechanisms, where the presence of nearby molecules makes it difficult to distinguish unimolecular from bimolecular processes and experimental interpretations of the initial events seem hopeless because the observed products may be the result of several sequential steps.

This paper is aimed at addressing this issue of determining the initial steps of solid phase reactions. We chose here to examine an energetic material since such systems are much easier to initiate experimentally, making it more likely that an experimentalist might be able to test our predictions. Our previous studies of bulk phase reactions used the ReaxFF reactive force field to follow the details of the reaction sequences at realistic reaction temperatures and pressures.[4,17–20] Indeed, these studies have received some overall confirmation from experiment, but only quantum mechanics (QM) can provide the full detailed mechanistic understanding of the initial reaction steps.

Thus, we report here Density Function Theory (DFT) studies of di-tetrazine-tetroxide (DTTO) crystals, an energetic material that has long been the target of synthetic attempts, because it was estimated to have a high density (up to 2.3 g cm^{-3}) and a performance substantially better than traditional EMs (such as RDX, HMX and CL-20), DTTO was seen as the performance limit for C-H-N-O explosives, making it a 'holy grail' in high-energy materials.

[a]Materials and Process Simulation Center, California Institute of Technology, Pasadena, California 91125, USA. E-mail: wag@wag.caltech.edu

[b]Key Laboratory of Soft Chemistry and Functional Materials of MOE, School of Chemical Engineering, Nanjing University of Science and Technology, Nanjing 210094, P. R. China

† Electronic supplementary information (ESI) available: Coordinates for structure of c1-$P2_12_12_1$ and c2-*Pbca* DTTO, studied supercell of c1-$P2_12_12_1$ DTTO and c2-*Pbca* DTTO, and atomic coordinates of all intermediates and TS shown in this study. See DOI: 10.1039/c4ta05676k

Previous first principles calculations used plane wave LDA density functional theory[22] to predict the most stable isomers of DTTO and the most favorable crystal packing mode. This led to a density of 2.0–2.3 g cm^{-3} and a velocity of detonation of $D_v = 10.9$ km s^{-1} confirming expectations that DTTO would be a high performance EM, in comparison $D_v = 8.75$ km s^{-1} for RDX, $D_v = 9.10$ km s^{-1} for HMX, and $D_v = 9.38$ km s^{-1} for CL-20.[21–24] However, LDA is not reliable for energies of molecular crystals.[25] So we report here studies using Density Functional Theory (DFT) at various levels (M06, B3LYP, PBE-ulg) which was used to examine the 20 possible isomers of DTTO. Then Monte Carlo sampling combined with UFF and Dreiding classical force fields was used to predict the best packings (*i.e.* polymorphs) among the 10 most common space groups for the two most stable isomers, c1 and c2. This was followed by DFT calculations at the PBE-ulg level to optimize the crystal packing.[26] We found that the most stable isomer c1 has the $P2_12_12_1$ space group with 4 molecules per cell (Fig. 1(a)), leading to a 1.96 g cm^{-3} density and a 301.9 kcal mol^{-1} detonation enthalpy (393.2 kcal mol^{-1} in ref. 23). The c2 isomer (less stable by 1.2 kcal mol^{-1}) has the *Pbca* space group with 8 molecules per cell (Fig. 1(b)) with a 1.98 g cm^{-3} density and a 302.4 kcal mol^{-1} (393.4 kcal mol^{-1} in ref. 23) detonation enthalpy.

In order to determine the energy release, detonation properties, and thermal stability of EMs, it is essential to determine the reaction mechanism for the initial reactions leading to thermal decomposition.[4,17,27–31] For such nitro-based EMs as TNT, RDX, and HMX the initial decomposition at low pressure is unimolecular NO_2 cleavage.[32–36] However for hydrogen containing high energetic materials such as RDX and HMX, Chakraborty *et al.*[3,27,31] used DFT to show that intramolecular hydrogen transfer to form HONO provides a completive first step of decomposition[37–40] that dominates under high pressure conditions.[41] Since DTTO has no hydrogen available to form HONO, its decomposition properties should be dramatically different (maybe better) than normal nitro-based explosives.

In this paper, we report the initial decomposition reaction mechanisms of DTTO using molecular dynamics simulations based on the PBE-ulg[42] flavor of DFT. The PBE-ulg corrects the poor description of van der Waals attraction (London dispersion) in PBE.[42] Here we consider stable monomers, c1 and c2 starting with their predicted most stable crystal structures ($P2_12_12_1$ for c1 and *Pbca* for c2).

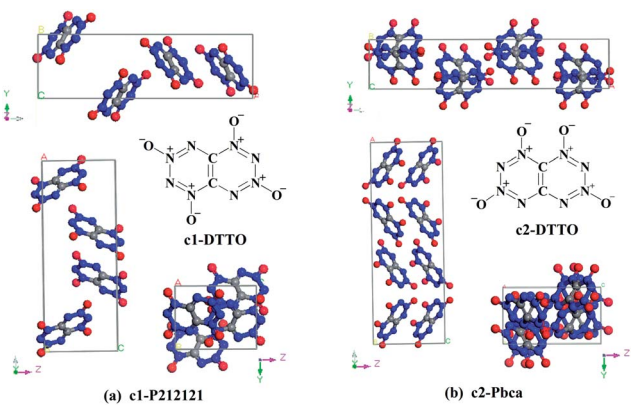

Fig. 1 Most stable molecular isomers di-tetrazine-tetroxide (DTTO), c1 and c2, and their predicted crystal structures: $P2_12_12_1$ for c1- and *Pbca* for c2-predicted from previous DFT calculations.[22,26] The C, O, N are represented by grey, red, and blue balls, respectively.

2. Simulations and computational method

In these DFT based molecular dynamics (MD) simulations, the interatomic forces are calculated in the framework of DFT,[43,44] where exchange and correlation were treated with the generalized gradient approximation (GGA), using the functional form of PBE-ulg method.[42]

The condensed phase DFT calculations were performed using VASP package.[45–48] For structure optimization we found that a kinetic energy cut-off of 500 eV for the plane wave expansions gives excellent convergence of the total energies, energy differences, and structural parameters. The same energy cut-offs were used in the DFT-MD calculations. Reciprocal space was sampled using the Γ-centered Monkhorst-Pack scheme using only the gamma point for the supercell calculations. The convergence criteria were set to a 1×10^{-6} eV energy difference for solving the electronic wave function and a 1×10^{-3} eV Å^{-1} force for geometry optimization. They were set to 1×10^{-5} eV energy difference for solving the electronic wave function and a 1×10^{-3} eV Å^{-1} force for DFT-MD simulation.

Two DTTO crystalline (c1-$P2_12_12_1$ and c2-*Pbca*) phases were considered in the DFT-MD simulations. Both consist of 16 molecules and were obtained by replicating the unit cell twice along the *y* and *z* directions for c1-$P2_12_12_1$, and twice along the *y* direction for c2-*Pbca*, respectively. Then the structures for the supercells were optimized individually before molecule dynamics simulations. The two initial structures of c1-$P2_12_12_1$ and c2-*Pbca* supercell are shown in Fig. S1.†

The procedure for the DFT-MD simulations was as follows: first the systems were heated from 20 K to 300 K over a period of 2 ps and then equilibrated at 300 K for 1 ps using the NVT (constant volume, constant temperature and constant number of atoms) ensemble. Finally, we heated the system from 300 K to 3000 K uniformly over the period of 20 ps. The time constant for the Nose–Hoover thermostat was 0.1 ps. We used a time step of 1 fs for integrating the equations of motion. To analyze the fragments during the simulation, we used a bond length cut-off of 1.5 times of the normal bond length. The actual bond lengths cut-offs are shown in the Table S1.†

To analyze the mechanisms for the reactions discovered during the simulations, we extracted the molecules undergoing a reaction from the DFT-MD trajectories and then carried out free molecule calculations to locate the nearby transition state for gas phase reactions at the level of PBE-ulg/6-31++G**. The Transition states (TS) were validated to have only one negative eigenvalue for Hessian. This was followed by intrinsic reaction coordinate (IRC) scans to connect the nearby reactant and the product structures.[49] To obtain free energies, we evaluated the thermodynamic properties were at 298.15 K and 1 atm. All gas phase calculations were carried out using the Jaguar 8.2 package.[50]

3. Results and discussion

The first-principle molecular dynamic simulation in this paper provides a very detailed, molecular-level description of the decomposition and reaction of DTTO in condensed phases under various conditions. Such information should allow one to extract valuable information about the complex chemistry involved, including uni- and multi-molecular reactions.[17] Our goal is to elucidate the initial reaction pathway as DTTO decompose and describe the events in this 'holy grail' of high-energy materials as it evolves to form intermediates that react with each other and with reactant to form eventually the final products observed theoretically. In this work, we focus on thermal decomposition of two most stable predicted DTTO crystals, c1-$P2_12_12_1$ and c2-*Pbca*, and examine the initial reaction details under various conditions.

3.1 Non-compressed c1-$P2_12_12_1$ DTTO

We first examined the initial decomposition reaction of c1-$P2_12_12_1$ DTTO. Fig. S1† shows the simulated system, which consists of 16 c1-DTTO molecules (224 atoms) in an 18.13 Å × 10.80 Å × 13.87 Å supercell.

The details of the DFT-MD studies are described below. Briefly we first equilibrate the structure at 300 K and then heat it at a uniform rate from 300 K to 3000 K over 20 ps. In our short time simulations (20 ps), no DTTO molecules decompose below 2000 K. Using the same computation approach (heating from 300 K to 3000 K over 20 ps) the decomposition temperature for beta-HMX is ~1850 K. This can be compared to the experimental thermal decomposition temperature for HMX of 548 K.[24] Based on this comparison, we estimate that the experimental thermal decomposition temperature for c1-$P2_12_12_1$ DTTO is ~615 K (similarly the results below suggest that for c2-*Pbca* the decomposition temperature is 790 K).

As shown in Fig. 2(a), for c1-DTTO we found that the first reaction at ~13.2 ps (T = 2100 K) is a unimolecular fragmentation of one DTTO molecule to form two N_2O molecules. About 0.1 ps later, additional DTTO molecules decompose, leading to the release of additional N_2O molecules.

To understand the nature of this first reaction of c1-$P2_12_12_1$ DTTO at ~13.2 ps (T = ~2100 K), we extracted the activated intermediate from the condensed phase simulation and analyzed the reaction mechanism as a gas phase unimolecular reaction. As described below we found the nearby transition state (TS) that has a single saddle point and then minimized to find the nearby stable reactant and product species. The observed reactions and the enthalpy of each species calculated in gas phase are shown in Fig. 3 and discussed below in detail.

We find that the unimolecular decomposition starts with breaking N–N and C–N bonds simultaneously to release the first N_2O *via* **TS1** with a 45.9 kcal mol^{-1} barrier. As the first N_2O leaves, the adjacent C forms a triple bond with its only neighbor N atom, driving the remaining 6-member ring to open to the intermediate **b** with 7.2 kcal mol^{-1} exothermicity. In this N_2O dissociation reaction, the pπ orbitals in resonance on O and N become singly-occupied sp^2 orbitals, resulting in a lone-pair on

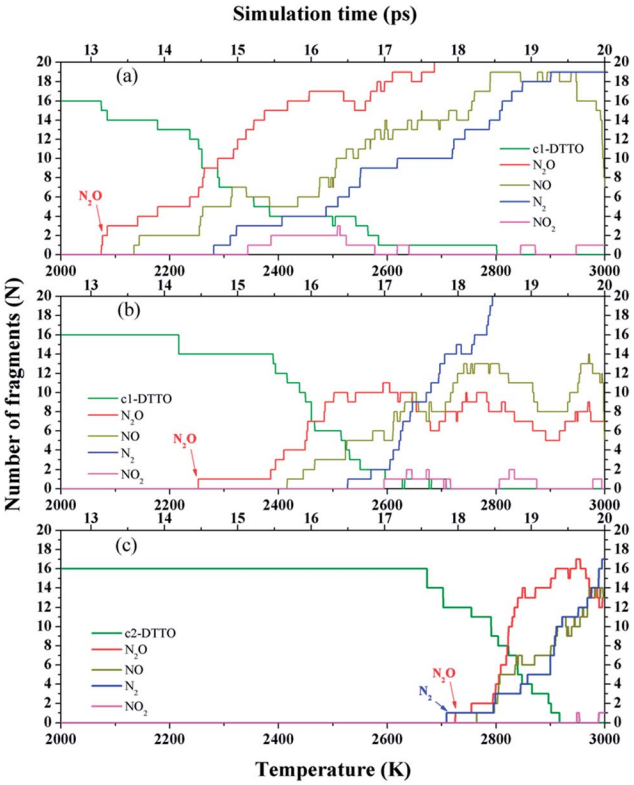

Fig. 2 Species analyses for the decomposition of (a) c1-$P2_12_12_1$ DTTO heated from 300 to 3000 K over 20 ps. At ~13.2 ps (T = 2100 K), the first DTTO molecule decomposes, releasing N_2O molecule. Starting ~0.1 ps later, DTTO molecules decompose one by one, releasing more N_2O molecules. (b) 30% uniaxial compressed c1-$P2_12_12_1$ DTTO is heated from 300 to 3000 K over 20 ps. At ~14.2 ps (T = 2250 K), two DTTO molecules react, to yield one N_2O product. At about 15.5 ps (T = ~2400 K), DTTO molecules start decomposing one by one, producing more N_2O molecules are also produced one by one (c) c2-*Pbca* DTTO heated from 300 to 3000 K over 20 ps. At ~17.5 ps (T = 2670 K), two DTTO molecules combine and 0.4 ps later, at ~17.9 ps (T = 2700 K), one N_2 molecule is released. At T = ~2700 K, one N_2O molecules was released.

N and an N=O double bond, as illustrated in the sub-view of Fig. 3. This mode of electron flow from π to σ is commonly observed in dissociation of N_2O from EMs, such as RDX or HMX.[27,31]

The next reactive step is to break the N–N bond *via* **TS2** to release the second N_2O with only a 6.4 kcal mol^{-1} barrier, leading to ring-closure with very high exothermicity (−55.0 kcal mol^{-1} from **b**). This is much greater than the −7.2 kcal mol^{-1} exothermicity of the first N_2O reaction that drives further decomposition of other DTTO molecules.

3.2 Compressed c1-$P2_12_12_1$ DTTO

It is generally accepted that the detonation starts at a hotspot that forms as the shock wave passes through.[51–53] Thus we also examined the mechanism of the initial reaction of c1-$P2_12_12_1$ DTTO compressed by 30% along the *a* direction (from *a* lattice constant of 18.13 Å to 12.69 Å) as shown in Fig. 4. This pre-compression leads to an initial external pressure of 15.9 GPa.

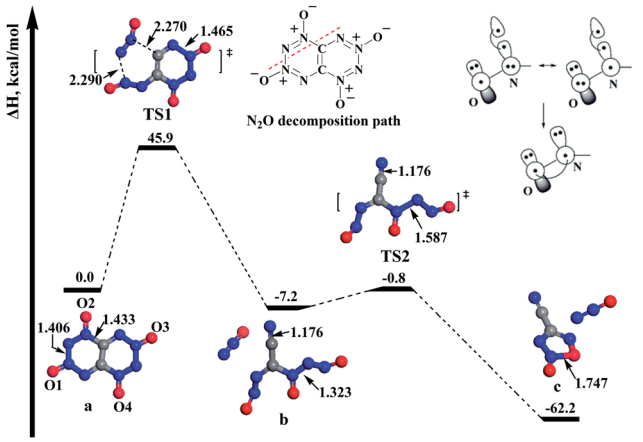

Fig. 3 Mechanism of c1-DTTO unimolecular decomposition obtained from gas phase calculations starting from the reactive intermediate extracted from the DFT-MD trajectory. This leads to release of two N_2O molecules. Configurations **TS1**, **TS2** and **c** are obtained from finite cluster DFT calculations.

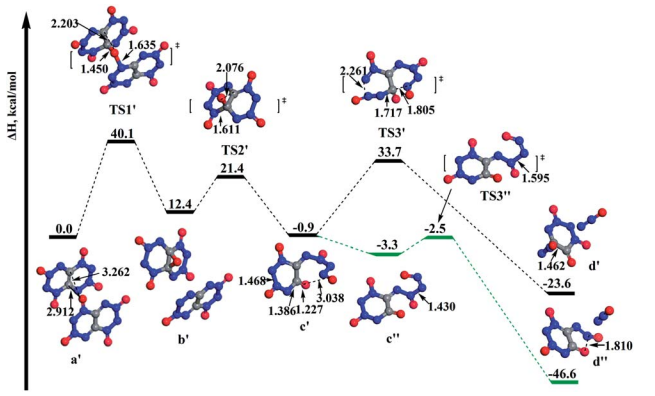

Fig. 5 The mechanism of the first bimolecular reaction for compressed c1-DTTO. First there is oxygen-transfer between the two DTTO molecules, which is followed quickly by N_2O release. Configurations **TS1′**, **TS2′** and **TS3′** were extracted from the DFT-MD trajectory and then optimized as a gas phase reaction. Path **c″**–**TS3″**–**d″** releases one N_2O, but was not observed in the DFT-MD simulations, we find a negligible barrier in the gas phase. The energies for these species involved in the decomposition sequence were calculated by finite cluster DFT calculations.

Then we built a 1 × 2 × 2 supercell containing 16 molecules and 224 atoms, as shown in Fig. S1(b).† Next we carried out DFT-MD as above, leading to the results in Fig. 2(b). Here the c1-DTTO molecules start to react at ~14.2 ps ($T = 2250$ K), with two DTTO molecules reacting to form new covalent bonds while releasing one N_2O product. Thus the initial reaction in the compressed system is not unimolecular.

Analyzing the reaction mechanism for just the bimolecular reaction of compressed c1-$P2_12_12_1$ DTTO, we found that this first reaction starts an oxygen-transfer between the two adjacent DTTO molecules, which is quite different from the mechanism in RDX and HMX EMs in which hydrogen-transfer to from HONO takes places at the beginning.[27,54,55]

As shown in Fig. 5, this bimolecular reaction involves three steps. The first step is the oxygen-transfer to make DTTO–epoxide *via* **TS1′**, in which one oxygen atom of c1-DTTO reacts with the C atom of the nearby DTTO to make the first C–O bond, followed by breaking the N–O bond and formation of the epoxide intermediate **b′**. This reaction is the rate-determining step (RDS) with a 40.1 kcal mol^{-1} barrier, which is 5.8 kcal mol^{-1} lower than the unimolecular N_2O-release reaction in uncompressed c1-$P2_12_12_1$ DTTO.

The second step starts with the ring-opening reaction of the epoxide (**TS2′**), which then form a new C=O double bond that drives the opening of the other 6-member ring to the intermediate **c′**. This reaction has a 9.0 kcal mol^{-1} barrier and releases an enthalpy of 13.3 kcal mol^{-1}. The third step to release N_2O observed in the MD simulation is *via* an S_N2-like mechanism in which the previously opened branch bounces back to form a 6-membered ring while releasing the N_2O on the other side, leading to a 34.6 kcal mol^{-1} barrier but with an exothermicity of 22.7 kcal mol^{-1} from **c′**. Starting with intermediate **c′**, we find a negligible barrier to first twist the opened branch and then stretch the N–N bond *via* **TS3″**. Despite the low gas phase barrier, this twist motion of the opened branch takes considerable free space so that it would be hindered by nearby DTTO molecules in the condensed phase, explaining why it was not observed in the MD simulation with its fast heating rate.

After the initial reaction at 14.2 ps, we found that at 15.5 ps (T = 2400 K), a number of N_2O molecules are released *via* unimolecular pathways, while the number of intact c1-DTTO molecules decreases one by one as shown in Fig. 6. This N_2O elimination is *via* **TS4′** at 43.3 kcal mol^{-1}, which gives a heterobicyclic ring **f′** with reaction enthalpy of −23.9 kcal mol^{-1}.

For c1-DTTO, we find a different reaction mechanism for the non-compressed state compared to the highly compressed state. For compressed c1-DTTO, the initial reaction involves an intermolecular oxygen migration, not the unimolecular reaction to release N_2O found for the non-compressed state. This oxygen migration reaction for the compressed case has a reaction barrier 5.8 kcal mol^{-1} lower than the N_2O releasing reaction.

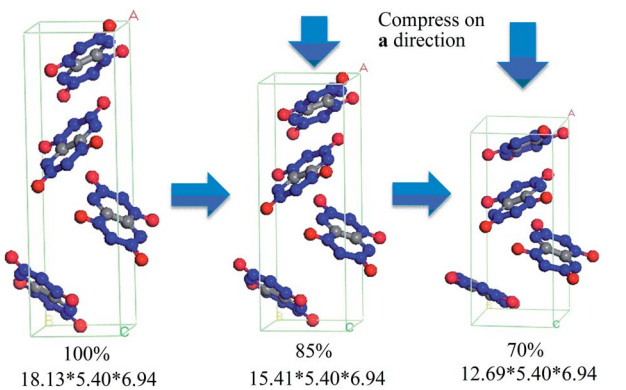

Fig. 4 Later view of 30% volume compression in *a* direction of c1-$P2_12_12_1$ DTTO unit cell. First compress the unit cell 15% and then go on compress it to 30%. Lattice constants are in Å.

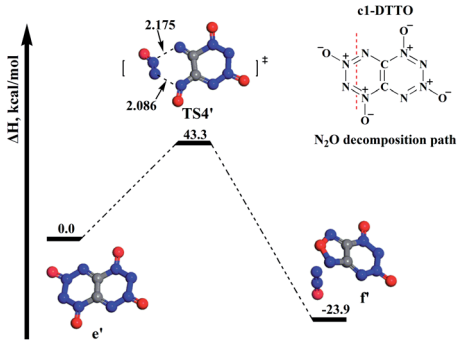

Fig. 6 Proposed mechanism of the N_2O elimination reaction in one c1-DTTO molecule. Configurations TS4′ and f′ are revealed by QM molecular dynamic simulations, and calculate accurate energies for these species involved in the decomposition sequence by DFT calculations.

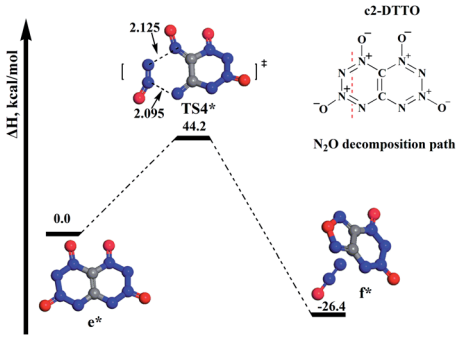

Fig. 8 Proposed mechanism of the N_2O elimination reaction in one c2-DTTO molecule. Configurations TS4* and f* are revealed by QM molecular dynamic simulations, and calculate accurate energies for these species involved in the decomposition sequence by DFT calculations.

This result suggests that external shock compression can affect on the decomposition pathway of energetic materials.

3.3 Non-compressed c2-*Pbca* DTTO

We then examined the initial decomposition mechanism for the c2 molecular isomer, which has the *Pbca* space group. Fig. 2(c) shows the number of N_2O, NO, N_2, and NO_2 fragments observed at temperatures ranging from 2000 K to 3000 K (no DTTO molecules decompose below 2000 K), corresponding to 16 ps to 20 ps.

For c2-DTTO we found that the first reactions start at 2670 K (~17.5 ps), involving the intermolecular reaction of two c2 molecules, with no gas products released. Then about 0.4 ps later, at ~17.9 ps ($T = 2700$ K), one N_2 molecule is released from this bimolecular complex. About 0.1 ps later ($T = \sim 2700$ K), one N_2O molecule was also released. This shows that by 2700 K, the primary reactions involve both N_2 and N_2O releasing processes. This is quite different from the c1 reaction mechanisms, in which the initial reactions involve unimolecular decomposition or oxygen transfer.

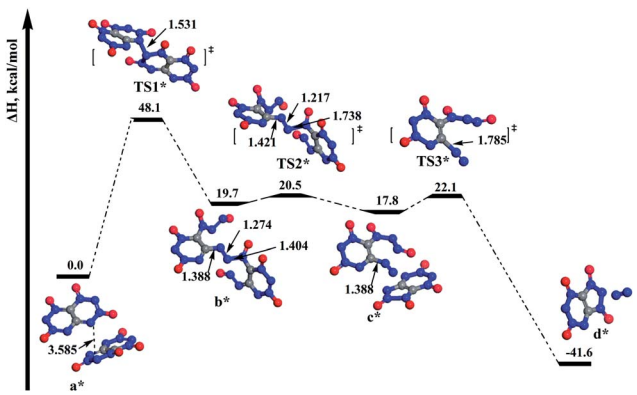

Fig. 7 Mechanism from QM molecular dynamic simulations by which two c2-DTTO molecules combine to release N_2. Configurations TS1*, TS2*, c* and d* are from by QM molecular dynamic simulations, and calculate accurate energies for these species involved in the decomposition sequence by DFT calculations.

Using QM we analyzed the reaction mechanism for the c2-DTTO bimolecular combination reaction at ~17.5 ps (~2600 K). As for the c1 case we searched first for the nearby transition state and then minimized to find the stable reactant and product structures. We find that first an N–N bond is formed between the two reacted DTTO molecules and then a new intermediate product appears. As the reaction proceeds, another N–N bond is broken in the newly formed intermediate leading to two new fragments. Then a C–N bond breaks in one of the newly formed fragments, releasing N_2, while simultaneously an N_2O molecule is released in a unimolecular reaction. The mechanism derived including the enthalpy for each species is shown in Fig. 7 for the case of N_2 releasing reaction and in Fig. 8 for the case of N_2O releasing reaction.

As shown in Fig. 7, this N_2 releasing mechanism also involves three steps. The first step is to form an N–N bond between two c2-DTTO molecules *via* **TS1*** with a 48.1 kcal mol^{-1} barrier, making it the rate determining step. This reaction opens a 6-member ring on each DTTO leading to a dimer **b*** connected with an azo bridge that is 19.7 kcal mol^{-1} endothermic. The azo group is then released from the DTTO dimer as a free N_2 by breaking N–N and N–C bonds sequentially *via* **TS2*** and **TS3*** with low barriers (<5 kcal mol^{-1}) to the product **d***. This very exothermic reaction ($\Delta H = -41.6$ kcal mol^{-1} *versus* **a***) leads to the decomposition of other DTTO molecules, just 0.1 ps after the first reaction, with one N_2O molecules released. As shown in Fig. 8, this N_2O elimination proceeds *via* **TS4*** with 44.2 kcal mol^{-1}, which similar to the N_2O elimination reaction shown in Fig. 6 except for the position of the breaking bonds.

4. Conclusions

In summary, these DFT molecular dynamics simulations provide a very detailed, molecular-level description of the initial decompositions and reactions of condensed phase DTTO under various conditions. This allows information about the complex chemistry involved to be extracted, including unimolecular and multimolecular reactions sequences.[17]

The goal in this paper was to examine the initial reaction pathway as DTTO decomposes to discover the events in this 'nitrogen-rich energetic material' as it evolves to form intermediates that react with each other and with reactant to eventually form the final products observed theoretically and experimentally.

We found three major initial reaction routes, depending upon temperature, pressure, and crystalline structure conditions:

(1) The first decomposition reaction of uncompressed c1-$P2_12_12_1$ DTTO is a unimolecular reaction that releases two N_2O molecules, with an enthalpic barrier of 45.9 kcal mol^{-1} and an exothermicity of 6.4 kcal mol^{-1} (PBE-ulg).

(2) As c1-$P2_12_12_1$ DTTO is compressed, the initial reaction becomes intermolecular transfer an oxygen atom from one c1 molecule to the nearest carbon of another, leading to an enthalpic barrier of 40.1 kcal mol^{-1}.

(3) For c2-*Pbca* DTTO, the decomposition reaction mechanism involves first combining two DTTO molecules and then releasing an N_2 molecule, leading to a reaction barrier of 48.1 kcal mol^{-1}.

These results suggest that a variety of initial decomposition reactions are favorable for DTTO, depending on temperature, pressure, and crystal packing. The c2-*Pbca* DTTO reaction begins at 300 K higher than c1-$P2_12_12_1$ but leads to bimolecular N_2 release, of twice the energy as for the unimolecular N_2O releasing reaction. This suggests that the thermal stability for c2-*Pbca* DTTO is higher than for c1-$P2_12_12_1$ DTTO. Thus the c2-*Pbca* could have better performance than c1 DTTO crystal.

The reaction barriers of 45.9 kcal mol^{-1} and 48.1 kcal mol^{-1} found for c1 and c2 DTTO are higher than the 39.0 kcal mol^{-1} NO_2 dissociation barrier for RDX, the 39.8 kcal mol^{-1} NO_2 dissociation barrier of for HMX and the 37.6 kcal mol^{-1} N–NO_2 homolysis reaction barrier of CL-20,[27,31,56] and the simulated initial decomposition temperatures are 200 K or more higher than beta-HMX by the same computational method. Thus we expect that DTTO may be a high performance explosive with higher thermal stability.

We expect these theoretical studies of the initial reaction of DTTO might stimulate further experimental studies of DTTO, particularly the synthesis, and characterization.

Acknowledgements

We thank Dr Cliff Bedford and Dr Al Stern for suggesting the importance of this work. All computations were carried out on the Army HPC systems; we thank Betsy Rice and Larry Davis for assistance. Personnel were supported mostly by ONR (N00014-09-1-0634, Cliff Bedford), with some assistance from ARO (W911NF-05-1-0345 and W911NF-08-1-0124). C.-C. Ye was sponsored by the China Scholarship Council (CSC), and thanks the Innovation Project for Postgraduates in Universities of Jiangsu Province (Grant no. CXZZ13_0213).

Notes and references

1 H. Xiao, Q. An, W. A. Goddard III, W. G. Liu and S. V. Zybin, *Proc. Natl. Acad. Sci. U. S. A.*, 2013, **110**, 5321–5325.
2 A. Hammerl, T. M. Klapotke, H. Noth, M. Warchhold, G. Holl, M. Kaiser and U. Ticmanis, *Inorg. Chem.*, 2001, **40**, 3570–3575.
3 D. Chakraborty, R. P. Muller, S. Dasgupta and W. A. Goddard III, *J. Comput.-Aided Mater. Des.*, 2002, **8**, 203–212.
4 A. Strachan, E. M. Kober, A. C. van Duin, J. Oxgaard and W. A. Goddard III, *J. Chem. Phys.*, 2005, **122**, 54502.
5 W. G. Liu, S. Q. Wang, S. Dasgupta, S. T. Thynell, W. A. Goddard III, S. Zybin and R. A. Yetter, *Combust. Flame*, 2013, **160**, 970–981.
6 O. Bolton and A. J. Matzger, *Angew. Chem., Int. Ed.*, 2011, **50**, 8960–8963.
7 D. C. Clary, *Proc. Natl. Acad. Sci. U. S. A.*, 2008, **105**, 12649–12653.
8 M. L. McKee, H. P. Reisenauer and P. R. Schreiner, *J. Phys. Chem. A*, 2014, **118**, 2801–2809.
9 R. T. Skodje, *Adv. Quantum Chem.*, 2012, **63**, 119–163.
10 L. D. McPherson, M. Drees, S. I. Khan, T. Strassner and M. M. Abu-Omar, *Inorg. Chem.*, 2004, **43**, 4036–4050.
11 D. R. Kent, N. Dey, F. Davidson, F. Gregoire, K. A. Petterson, W. A. Goddard III and J. D. Roberts, *J. Am. Chem. Soc.*, 2002, **124**, 9318–9322.
12 D. R. Kent, K. A. Petterson, F. Gregoire, E. Snyder-Frey, L. J. Hanely, R. P. Muller, W. A. Goddard III and J. D. Roberts, *J. Am. Chem. Soc.*, 2002, **124**, 4481–4486.
13 V. R. Ziatdinov, J. Oxgaard, O. A. Mironov, K. J. H. Young, W. A. Goddard III and R. A. Periana, *J. Am. Chem. Soc.*, 2006, **128**, 7404–7405.
14 O. A. Mironov, S. M. Bischof, M. M. Konnick, B. G. Hashiguchi, V. R. Ziatdinov, W. A. Goddard III, M. Ahlquist and R. A. Periana, *J. Am. Chem. Soc.*, 2013, **135**, 14644–14658.
15 A. V. Sberegaeva, W. G. Liu, R. J. Nielsen, W. A. Goddard III and A. N. Vedernikov, *J. Am. Chem. Soc.*, 2014, **136**, 4761–4768.
16 W. G. Liu, A. V. Sberegaeva, R. J. Nielsen, W. A. Goddard III and A. N. Vedernikov, *J. Am. Chem. Soc.*, 2014, **136**, 2335–2341.
17 S. P. Han, A. C. van Duin, W. A. Goddard III and A. Strachan, *J. Phys. Chem. B*, 2011, **115**, 6534–6540.
18 N. Rom, B. Hirshberg, Y. Zeiri, D. Furman, S. V. Zybin, W. A. Goddard III and R. Kosloff, *J. Phys. Chem. C*, 2013, **117**, 21043–21054.
19 L. C. Liu, C. Bai, H. Sun and W. A. Goddard III, *J. Phys. Chem. A*, 2011, **115**, 4941–4950.
20 L. Z. Zhang, S. V. Zybin, A. C. T. van Duin, S. Dasgupta, W. A. Goddard III and E. M. Kober, *J. Phys. Chem. A*, 2009, **113**, 10619–10640.
21 H. Östmark, S. Wallin and P. Goede, *Cent. Eur. J. Energ. Mater.*, 2007, **4**, 83–108.
22 X. L. Song, J. C. Li, H. Hou and B. S. Wang, *J. Comput. Chem.*, 2009, **30**, 1816–1820.

23 P. Politzer, P. Lane and J. S. Murray, *Cent. Eur. J. Energ. Mater.*, 2013, **10**, 37–52.
24 D. Klasovity, S. Zeman, A. Ruzicka, M. Jungova and M. Rohac, *J. Hazard. Mater.*, 2009, **164**, 954–961.
25 K. R. Jorgensen and A. K. Wilson, *J. Comput. Chem.*, 2012, **33**, 1967–1968.
26 J. L. Mendoza-Cortes, Q. An, W. A. Goddard III, C. Ye and S. V. Zybin, *J. Comput. Chem.*, 2014, submitted.
27 D. Chakraborty, R. P. Muller, S. Dasgupta and W. A. Goddard III, *J. Phys. Chem. A*, 2000, **104**, 2261–2272.
28 N. Umezawa, R. K. Kalia, A. Nakano, P. Vashista and F. Shimojo, *J. Chem. Phys.*, 2007, **126**, 234702.
29 R. A. Fifer, in *Fundamentals of Solid-Propellant Combustion*, AIAA, New York, 1984.
30 M. R. Manaa, L. E. Fried, C. F. Melius, M. Elstner and T. Frauenheim, *J. Phys. Chem. A*, 2002, **106**, 9024–9029.
31 D. Chakraborty, R. P. Muller, S. Dasgupta and W. A. Goddard III, *J. Phys. Chem. A*, 2001, **105**, 1302–1314.
32 S. N. Bulusu, in *Chemistry and physics of energetic materials*, Kluwer Academic, Boston Norwell, MA, U.S.A., 1990.
33 C. J. Wu and L. E. Fried, *J. Phys. Chem. A*, 1997, **101**, 8675–8679.
34 K. K. Irikura, *J. Phys. Chem. A*, 2013, **117**, 2233–2241.
35 R. Cohen, Y. Zeiri, E. Wurzberg and R. Kosloff, *J. Phys. Chem. A*, 2007, **111**, 11074–11083.
36 X. F. Chen, J. F. Liu, Z. H. Meng and K. L. Han, *Theor. Chem. Acc.*, 2010, **127**, 327–344.
37 B. Wang, D. Wright, D. Cliffel, R. Haglund and S. T. Pantelides, *J. Phys. Chem. A*, 2011, **115**, 8142–8146.
38 D. Furman, R. Kosloff, F. Dubnikova, S. V. Zybin, W. A. Goddard III, N. Rom, B. Hirshberg and Y. Zeiri, *J. Am. Chem. Soc.*, 2014, **136**, 4192–4200.
39 C. A. Mayhew, P. Sulzer, F. Petersson, S. Haidacher, A. Jordan, L. Mark, P. Watts and T. D. Mark, *Int. J. Mass Spectrom.*, 2010, **289**, 58–63.
40 Z. Takats, I. Cotte-Rodriguez, N. Talaty, H. W. Chen and R. G. Cooks, *Chem. Commun.*, 2005, 1950–1952.
41 A. Strachan, A. C. van Duin, D. Chakraborty, S. Dasgupta and W. A. Goddard III, *Phys. Rev. Lett.*, 2003, **91**, 098301.
42 H. Kim, J. M. Choi and W. A. Goddard III, *J. Phys. Chem. Lett.*, 2012, **3**, 360–363.
43 W. Kohn and L. J. Sham, *Phys. Rev.*, 1965, **140**, 1133–1138.
44 P. Hohenberg and W. Kohn, *Phys. Rev. [Sect.] B*, 1964, **136**, B864–871.
45 G. Kresse, *J. Non-Cryst. Solids*, 1995, **193**, 222–229.
46 G. Kresse and J. Furthmuller, *Comput. Mater. Sci.*, 1996, **6**, 15–50.
47 G. Kresse and J. Furthmuller, *Phys. Rev. B: Condens. Matter Mater. Phys.*, 1996, **54**, 11169–11186.
48 G. Kresse and D. Joubert, *Phys. Rev. B: Condens. Matter Mater. Phys.*, 1999, **59**, 1758–1775.
49 K. Fukui, *Acc. Chem. Res.*, 1981, **14**, 363–368.
50 A. D. Bochevarov, E. Harder, T. F. Hughes, J. R. Greenwood, D. A. Braden, D. M. Philipp, D. Rinaldo, M. D. Halls, J. Zhang and R. A. Friesner, *Int. J. Quantum Chem.*, 2013, **113**, 2110–2142.
51 F. P. Bowden and A. D. Yoffe, in *Initiation and Growth of Explosions in Liquids and Solids*, Cambridge University Press, Cambridge, UK, 1952.
52 Q. An, S. V. Zybin, W. A. Goddard III, A. Jaramillo-Botero, M. Blanco and S. N. Luo, *Phys. Rev. B*, 2011, **84**, 220101.
53 Q. An, W. A. Goddard III, S. V. Zybin, A. Jaramillo-Botero and T. T. Zhou, *J. Phys. Chem. C*, 2013, **117**, 26551–26561.
54 L. M. Minier, K. R. Brower and J. C. Oxley, *J. Org. Chem.*, 1991, **56**, 3306–3314.
55 L. L. Davis and K. R. Brower, *J. Phys. Chem.*, 1996, **100**, 18775–18783.
56 S. Okovytyy, Y. Kholod, M. Qasim, H. Fredrickson and J. Leszczynski, *J. Phys. Chem. A*, 2005, **109**, 2964–2970.

